III. THICKNESS EXCITATION OF THICKNESS MODES

We begin by presenting the analytic solution of the problem of thickness modes of an electroded, piezoelectric crystal plate with traction-free surfaces, driven by an electric field in the thickness direction (64,65), after which we synthesize exact network equivalents using transmission lines. Then, with a view to removing the restriction to traction-free boundaries, the electromechanical impedance matrix is determined in the normal coordinate system. This matrix is then realized rigorously, in transmission-line circuit form. When taken together with the network developments presented in Chapter V, the TETM problem for a single plate with arbitrary boundary-port conditions becomes completely represented by the overall network, which is a true analog of the physical situation.

A. Single-Plate Crystal Resonator, Traction-Free.

Our plate is presumed to be laterally unbounded, of thickness 2h, the upper and lower surfaces at $x_3 = +h$ and $-h$, respectively, are further presumed to be maintained at potentials $+\varphi_0$ and $-\varphi_0$, also respectively, the time factor $\exp(+j\omega t)$ being, as usual, suppressed. The electrodes for accomplishing this are not of interest now; let them simply be perfect electrical conductors, massless, and without elastic stiffness. A sketch of the situation is given in Fig. 8. The lateral coordinates are, likewise, of no interest now.

At the plate boundaries, the conditions to be satisfied are

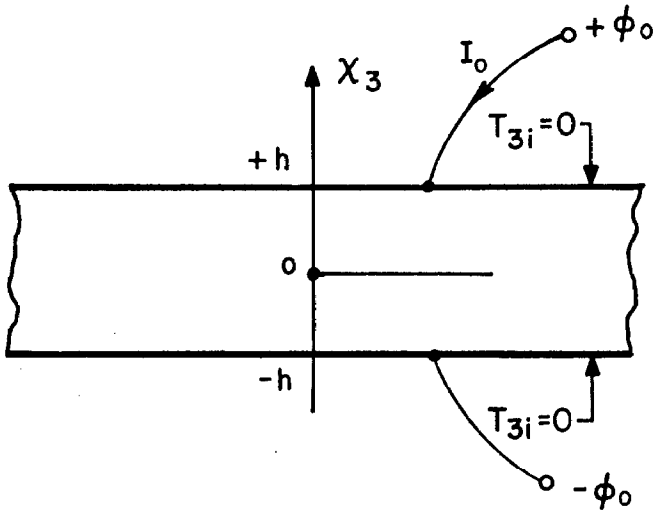

FIG 8. UNBOUNDED, TRACTION-FREE, PIEZOELECTRIC PLATE. THICKNESS EXCITATION OF THICKNESS MODES.

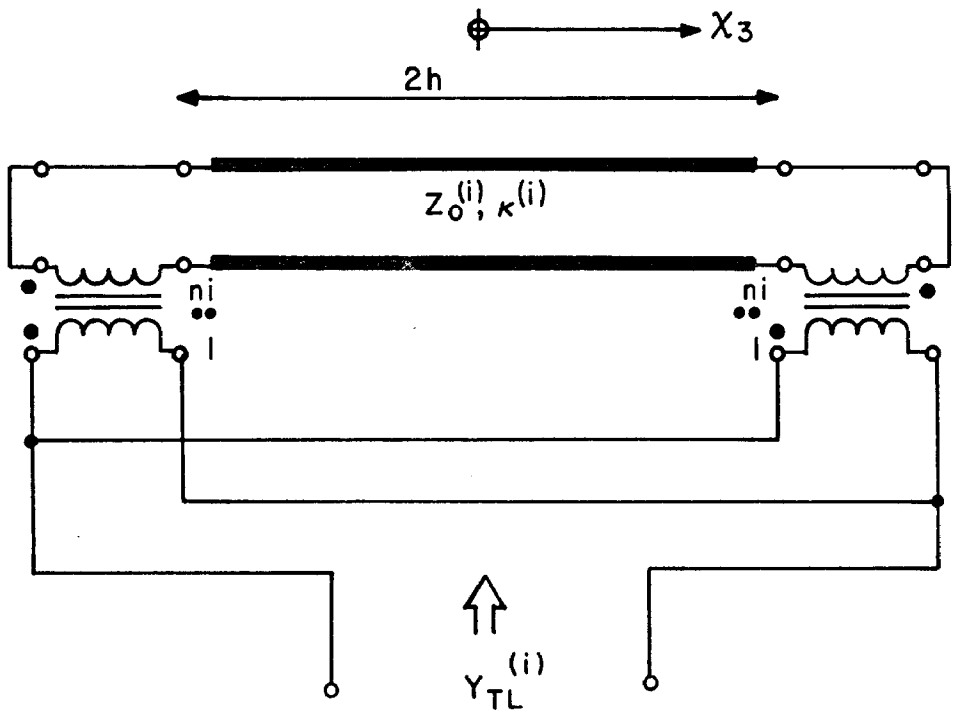

FIG. 9. TRACTION-FREE PLATE. REPRESENTATION OF SINGLE THICKNESS MODE, ELECTRICAL INPUT CIRCUIT OMITTED.

$$T_{3j} = 0 , \quad at \quad x_3 = \pm h , \tag{3.1}$$

and

$$\varphi = \pm \varphi_0 , \quad at \quad x_3 = \pm h . \tag{3.2}$$

Because the untransformed stresses T_{3j} vanish at the surfaces, the transformed stresses T°_{3j} also vanish:

$$T^{\circ}_{3i} = 0 , \quad at \quad x_3 = \pm h . \tag{3.3}$$

This is a consequence of (2.27) and the fact that $\beta_i^{(j)}$ is nonsingular; it has a determinant equal to unity.

We now seek a solution to (2.39) which satisfies the boundary conditions (3.2) and (3.3) when inserted into (2.41) and (2.38). In keeping with the symmetry of the problem, we select

$$u^{\circ}_i = U_i \sin \varkappa^{(i)} x_3 , \tag{3.4}$$

which satisfies (2.39), and put it into (2.38), using (3.3):

$$\begin{aligned} T^{\circ}_{3i} &= \mathcal{C}^{(i)} u^{\circ}_{i,3} + e^{\circ}_{33i} a_3 \\ &= \mathcal{C}^{(i)} \varkappa^{(i)} U_i \cos \varkappa^{(i)} h + e^{\circ}_{33i} a_3 \\ &= 0 \quad at \quad x_3 = \pm h , \end{aligned}$$

hence,

$$U_i = \frac{- e^{\circ}_{33i} a_3}{\mathcal{C}^{(i)} \varkappa^{(i)} \cos \varkappa^{(i)} h} . \tag{3.5}$$

The quantity a_3 is determined by substitution of (3.4) and (3.5) into (2.41) and using (3.2). This also fixes b_3 appearing

in (2.41). These manipulations result in

$$b_3 = 0 ,$$

and

$$a_3 = \frac{+ \varphi_o / h}{\left\{ 1 - \sum_{i=1}^{3} (k^{(i)})^2 \frac{\tan \varkappa^{(i)} h}{\varkappa^{(i)} h} \right\}} , \tag{3.6}$$

where

$$(k^{(i)})^2 = \frac{e^{\circ}_{3i3} \; e^{\circ}_{33i}}{\epsilon^{S}_{33} \; c^{(i)}} , \quad \text{(no sum)} \tag{3.7}$$

and $k^{(i)}$ is the piezoelectric coupling coefficient for mode (i) in the TEIM case. Because of the symmetry of the e°_{ijk}, the last two indices can be interchanged, so the numerator of (3.7) is simply the square of the appropriate transformed piezoelectric constant.

From the expressions given, one has

$$T^{\circ}_{3i} = e^{\circ}_{33i} \; a_3 \left\{ 1 - \frac{\cos \varkappa^{(i)} x_3}{\cos \varkappa^{(i)} h} \right\} , \quad \text{(no sum)} \tag{3.8}$$

and

$$u^{\circ}_i = \frac{- e^{\circ}_{33i} \sin \varkappa^{(i)} x_3}{c^{(i)} \varkappa^{(i)} h \cos \varkappa^{(i)} h} \cdot \frac{\varphi_o}{\left\{ 1 - \sum_{j=1}^{3} (k^{(j)})^2 \frac{\tan \varkappa^{(j)} h}{\varkappa^{(j)} h} \right\}} . \tag{3.9}$$

Equation (2.20) is

$$D_3 = - \epsilon^{S}_{33} \; a_3 , \tag{2.20}$$

therefore, we get

$$D_3 = \frac{-\epsilon_{33}^{S}\,\varphi_0/h}{\left\{1-\sum_{j=1}^{3}(k^{(j)})^2\,\frac{\tan x^{(j)}h}{x^{(j)}h}\right\}} \,. \tag{3.10}$$

Now consider a portion of the plate having lateral area A. This is the same area introduced in (2.52). The current, I_o, intercepted by this area, is equal to

$$I_o = -A\,\dot{D}_3 \,, \tag{3.11}$$

$$I_o = -j\omega A D_3 \,. \tag{3.12}$$

The minus sign is a consequence of the fact that, at the positive (upper) electrode, the surface normal points in the direction of minus x_3 within the crystal.

Looking into the electrical port, one sees an admittance

$$Y_{in\,(TETM)} = I_o/(2\varphi_o) \,, \tag{3.13}$$

with I_o given by (3.12).

Defining the capacitance Co by

$$C_o = A\,\epsilon_{33}^{S}/(2h) \,, \tag{3.14}$$

and using (3.10), (3.12) and (3.13), we arrive at the input admittance (65):

$$Y_{in\ (TETM)} = \frac{j\omega C_o}{\left\{1 - \sum_{p=1}^{3} (k^{(p)})^2 \frac{\tan \chi^{(p)} h}{\chi^{(p)} h}\right\}} . \qquad (3.15)$$

B. Network Synthesis of Y_{in} (TETM).

Expression (3.15), for the input admittance seen at the electrical port of the traction-free crystal plate, is a function of three tangents having, generally, different periods, since all the wavenumbers $\chi^{(p)}$ will usually be distinct. Remembering what was said earlier concerning the three acoustic eigen-modes satisfying transmission-line equations, and also the discussions in the Introduction about piezoelectric coupling of the modes at boundaries, and viewing (3.15) in this light, we might expect that (3.15) could be realized by a generalization of Fig. 7, involving three transmission lines. Such is indeed the case, and this simple problem has been selected here with just this end in mind. It will introduce a three-transmission-line network with the least amount of additional detail, so that the increased complexity will not obscure the ties our circuits have with those previously given in the literature.

To begin the synthesis, recall that Fig. 7 represents a mode driven by an applied field parallel to the wave propagation direction, which is also true in our case. Circuits for the field normal to the wave propagation, on the other hand, are distinguished in the literature (131) by the absence of the negative C_o. With this hint, we extract from Y_{in} (TETM) in (3.15) a shunt capacitor of value C_o, and then a series capacitor of value minus C_o. This fragment of the TETM network has been called the "electrical input

circuit" by Schüssler (143); we will retain the name.

When the electrical input circuit, described above, has been extracted from Y_{in} (TETM), the remainder, Y_{TL}, say, is

$$Y_{TL} = j\omega C_o \left\{ \sum_{p=1}^{3} (k^{(p)})^2 \frac{\tan \varkappa^{(p)} h}{\varkappa^{(p)} h} \right\}. \tag{3.16}$$

This means that we have the sum of three admittances in parallel, and each admittance contains one tangent function.

We next notice that, because of the mechanical boundary conditions, the surface stresses, both T_{3i} and T°_{3i}, vanish, while the corresponding displacements are allowed to develop freely. Equations (2.52) and (2.53) then suggest as a consequence that the mechanical ports are short circuited.

Let us first consider one of the three admittances comprising Y_{TL}, for if we can formulate an appropriate network for one of the three terms, we have only to add, in parallel, two others which are alike it save for the mode index number. Call this admittance $Y^{(i)}_{TL}$.

With Fig. 7 in mind, we are thus led to Fig. 9, wherein, to be consistent with Chapter II, we have used

$$Z^{(i)}_o = A \rho v^{(i)}, \tag{2.54}$$

$$\varkappa^{(i)} = \omega / v^{(i)}, \tag{2.45}$$

which then requires that the piezoelectric transformer turns ratios, n_i, become

$$n_i = + A e^{\circ}_{33i} / (2h), \tag{3.17}$$

and the transformer dots to be located as given. The fact that the dots are adjacent at one end, and opposite at the other end is a manifestation of the polar nature of the piezoelectric effect; the circuit is mechanically symmetric.

In drawing Fig. 9 with the transformers as shown, we emphasize the concept of boundary excitation. We have given in the figure a representation with the transformer primaries in parallel; one can as well redraw it with a single primary winding, and two secondary windings with a common flux, so that the secondaries are in parallel.

Figure 9 may be verified by reverting back to the equivalent tee circuit for a transmission line, as given, for example, in Fig. 4. We shall omit doing it here, and go on instead to the complete network, since we have accumulated all of the pieces. We require three networks as in Fig. 9, in parallel, plus the electrical input circuit, attached to the electrical port. Figure 10 shows the assembled network.

Equation (2.47) tells us that, because the T°_{3i} vanish at the plate surfaces, the partial stresses $\tilde{T}^{\circ}_{3i}$ and $\bar{T}^{\circ}_{3i}$ add to zero there. According to our discussions in Chapter II, $A\,\tilde{T}^{\circ}_{3i}$ are the voltage variables associated with the waves on the transmission lines, while the $A\,\bar{T}^{\circ}_{3i}$ are piezoelectric in nature, since

$$A\bar{T}^{\circ}_{3i} = A\,e^{\circ}_{33i}\,a_3, \tag{3.18}$$

which follows from (2.48). We see that Fig. 10 provides just these interpretations when the $A\,\bar{T}^{\circ}_{3i}$ are identified with the secondary voltages produced by the piezo-transformers located at the ends of the transmission lines.

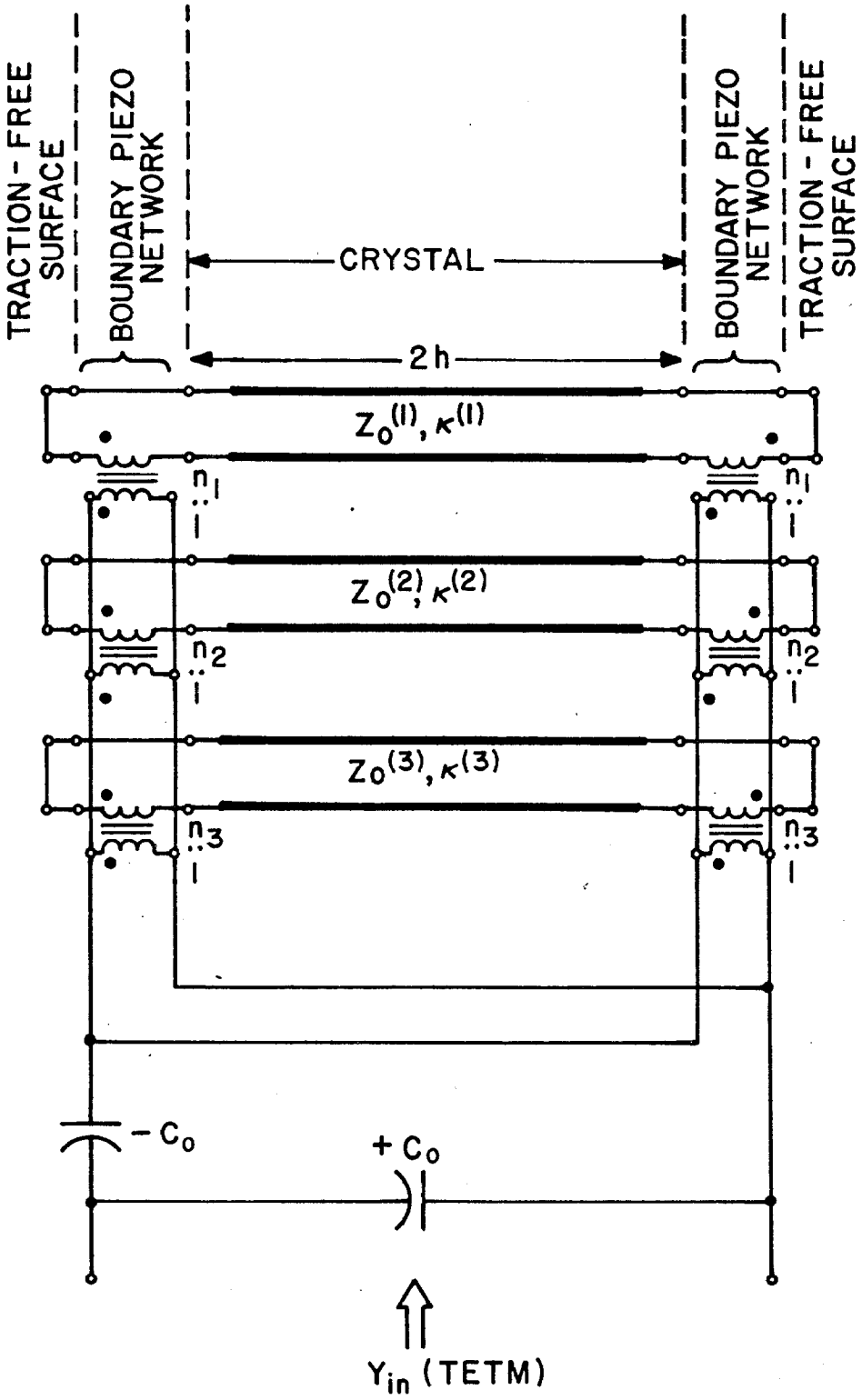

FIG. 10. EQUIVALENT NETWORK ANALOG REPRESENTATION OF TRACTION-FREE PLATE, TETM.

The structure of Fig. 10 also furnishes a simple, visual, interpretation to Tiersten's finding (64) that, even in the traction-free case, all three modes are coupled, piezoelectrically, at the boundary. It is clear that, if the electrical port is left open, the positive and negative capacitors combine to short-circuit the piezotransformers, and the three eigen-modes are then decoupled. In any other case, where the electrical port is attached to a finite immittance, the three modes are boundary-coupled.

Other insights may be obtained through a study of the schematic, but it is not our intent to be exhaustive about this aspect of the problem; we desire to derive networks which are rigorously analogous to the problems stated, and make a few observations about them. Once they are understood, and some facility is obtained in manipulating them, they speak for themselves.

We will confine ourselves, now, to the following remarks in regard to Fig. 10 and the physical problem it represents.

Equation (3.15) is an exact result, and Fig. 10 realizes it exactly. The figure, therefore, can be used for time-domain analyses, even though it was developed from a frequency-domain synthesis. Consider this aspect briefly. One can see that a transient excitation applied to the electrical port produces two waves in each transmission line, each wave starting at the surface and propagating inwardly. Each pair of waves is of equal strength and the stresses have the same polarity, so, consequently, no net mechanical current will flow across the center line of the resonator plate.

When two of the three piezoelectric turns ratios n_i are zero,

only a single transmission line remains coupled to the electrical input circuit, and, in this simpler case, the time-domain response reduces to that given in the literature (88, 99-101). If two n_i are zero, and only one mode is driven piezoelectrically, (3.15) shows that the critical frequencies, corresponding to poles and zeros of Y_{in} (TETM), are obtained from the roots of

$$\tan \varkappa h = \infty \,, \tag{3.19}$$

which gives the harmonically-related antiresonant frequencies, and from the roots of

$$\tan \varkappa h = +\varkappa h / k^2 \,, \tag{3.20}$$

which gives the non-harmonically-related resonant frequencies. Since only one mode is now considered, the mode superscript is dropped. Tiersten (64) has given a discussion of the meaning of (3.20); it was first derived by Bechmann (134), in 1940, for a single mode.

Reverting back to the case of three modes, the exact result (3.15) may be used down to DC in which limit the effective capacitance becomes

$$C_{DC} = \frac{C_o}{\left[1 - \sum_{p=1}^{3} (k^{(p)})^2 \right]} \,, \tag{3.21}$$

whereas, in the absence of piezoelectricity, the limit would be simply C_o. The piezo-coupling factors $k^{(p)}$ have the effect, therefore, of increasing the effective permittivity. This has been shown, also by Bechmann (200). Because the crystal plate is passive, moreover, it is necessary that the limiting capacitance at DC be positive,

which implies the constraint on the coupling factors

$$\sum_{p=1}^{3} (k^{(p)})^2 < 1 . \qquad (3.22)$$

Additional relations of this sort may be derived from the necessity that the stored energy density be positive. This, in turn, requires that the overall material constant matrix formed from (2.5) and (2.6) be positive definite (164), and leads to a variety of results. Some general considerations relating to coupling factors are given in the paper by Baerwald (201).

The network of Fig. 10 degenerates, at DC, into a simple capacitor circuit that consists of the TETM electrical input circuit (C_o in shunt, followed by $-C_o$ in series) and three capacitors in parallel, one for each transmission line, each of value $C_o(k^{(p)})^2$. In the high frequency limit the input capacitance approaches C_o, the piezoelectrically induced motion becoming "frozen."

We now use the symmetry of Fig. 10 to simplify it. Because of the transformer dot array, the mechanical voltages produced at the ends of each transmission line have the same polarity, as noted earlier, and the mid-point of the lines, corresponding to the plane $x_3 = 0$, of the crystal plate, is a node of mechanical current. We may therefore bisect the network of three transmission lines at their centers (19). The bisection produces six lines, each of length h, open circuited at the ends at which the bisections were made. The six lines consist of three sets of identical twins, which are all connected in parallel through their piezo-transformers. Each set of twin lines can be further reduced to a single line, having twice the characteristic admittance of the individual lines. Our manipulations lead us thus to Fig. 11.

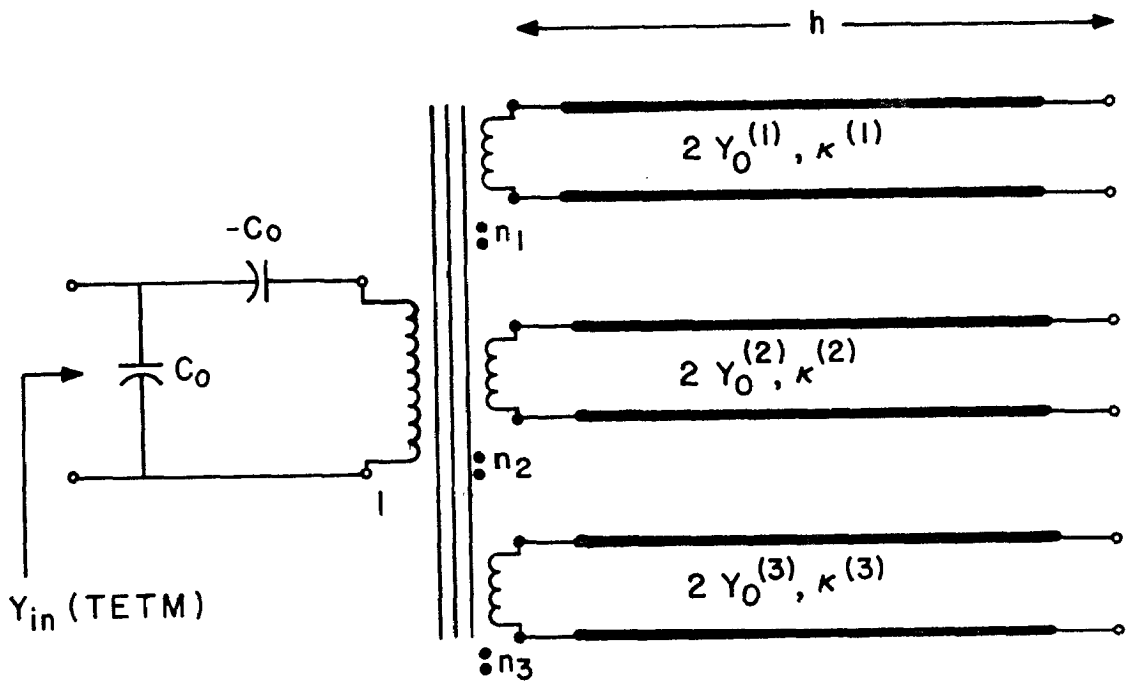

FIG. 11. EXACT EQUIVALENT NETWORK FOR TRACTION-FREE PLATE, TETM. BISECTED BASIS.

Here, the three modal transmission lines have been connected via a common core transformer, so that the secondaries are in parallel.

Although we have not shown it yet, Fig. 10 is a true analog representation where the vibrating plate parameters, such as the displacements, u_i , may be determined exactly as a function of coordinate x_3 , from a consideration of the network. Figure 11, on the other hand, has lost this intimate physical meaning, because of the circuit manipulations that have been carried out. The important thing to be emphasized will vary with the situation, usually; at first, the analogous aspects of the representations provide insight into the physics, while at a later stage, after insight has been attained, circuit simplifications can be sought to reduce the network configuration to more tractable forms for application.

We leave the one-port, traction-free plate now, and pass on to a more general treatment of the TETM-driven plate which will lead, in Chapter V, to a complete seven-port network for handling arbitrary boundary conditions.

C. The Electromechanical Network Impedance Matrix.

Our network of Fig. 10 realizes input admittance (3.15) exactly. It was obtained by a one-port synthesis, and no other constraints were imposed other than that (3.15) be satisfied. As we indicated toward the close of the last section, and this is significant, the network of Fig. 10 actually is valid on a point-to-point basis, and not simply valid only at the electrical port. Because this is so, it can be generalized to arbitrary boundary conditions, as we shall shortly show. The traction-free-boundary plate, chosen to introduce our new results because of its simplicity, led to the imposition of short circuits

at the mechanical ports; in more general instances the shorts will be replaced by mechanical boundary networks, coupling the three transmission lines to each other, and to the mechanical impedances, seen at the boundary, arising from adjacent strata, lumped loads, or other mechanical influences.

We thus anticipate the more general network of Fig. 12. The construction of the mechanical boundary networks will be given in Chapter V. In the figure the negative capacitance, associated with TETM, has been disposed symmetrically in the electrical input circuit, and placed more explicitly at the crystal interfaces, whereas the shunt capacitance is clearly associated with the crystal in the bulk. It is understood that the shunt capacitor plates coincide with the plate surfaces for a complete analog; they are drawn using the conventional circuit symbol as a convenience. We mention in passing that one may look upon this static capacitance C_o, as a vestige of the two electromagnetic modes in the quasi-static approximation, so that, additional to the three acoustic transmission lines, a fourth line exists, representing these two coalesced modes, the velocity on which line is infinite.

Our object here is twofold. We must provide a link between the traction-free case of Fig. 10 and the anticipated picture of Fig. 12 for general mechanical boundary conditions. At the same time, we must show these general circuit forms to be true analogs, i.e., we must investigate the correspondence of the picture with the spatial coordinate, and treat the network as a seven-port, rather than as a one-port, because the three stress and three displacement (or velocity) components at each of the two surfaces are generally interrelated.

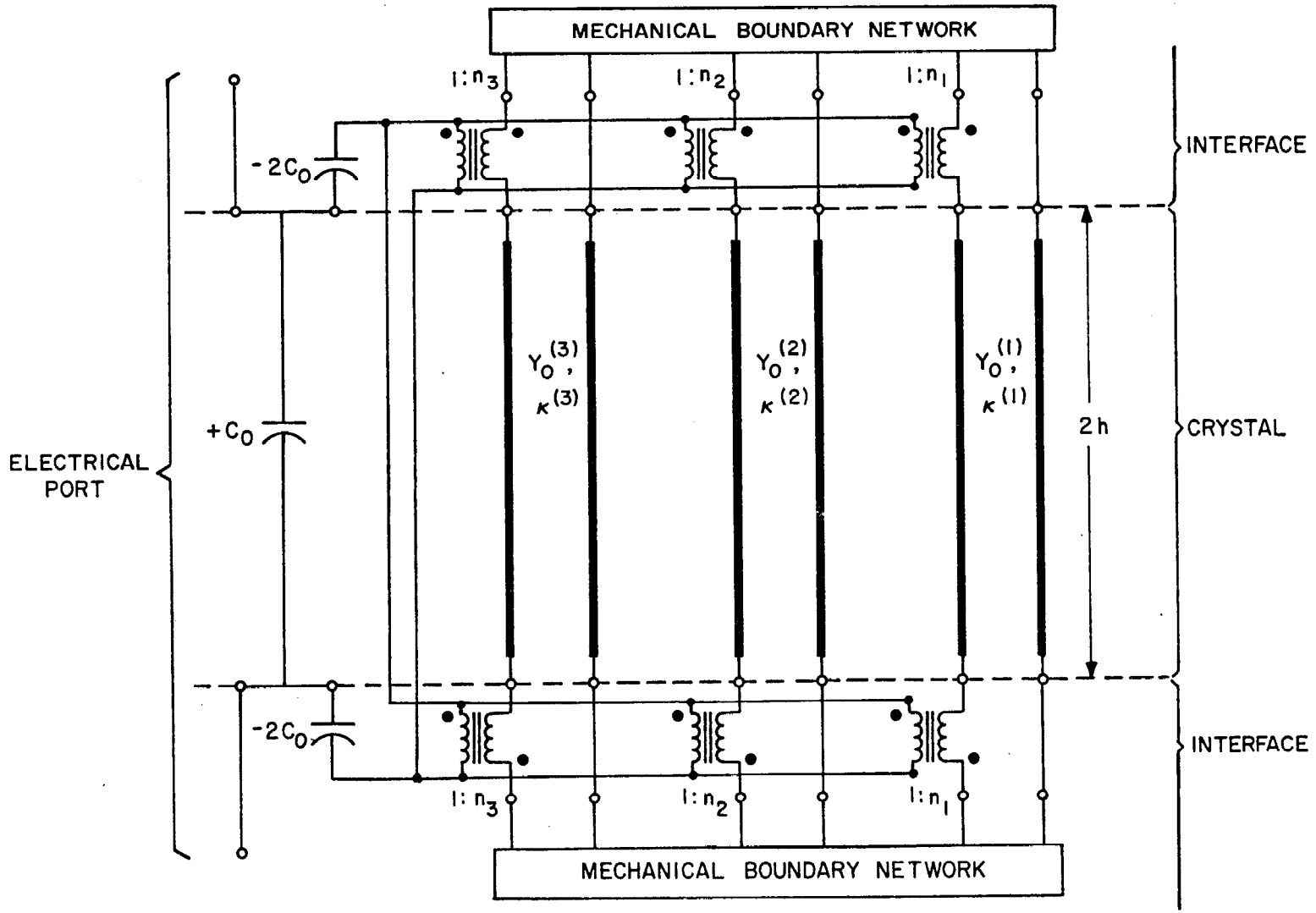

FIG. 12. EQUIVALENT NETWORK ANALOG REPRESENTATION OF TETM PLATE WITH ARBITRARY MECHANICAL BOUNDARY LOADINGS.

To accomplish these ends most easily, we take the following course. We will reverse our procedure of solving the physical problem first and then realizing its network, as we did in Sections III A and B above; instead we provisionally adopt the circuit of Fig. 13, examine it from a network standpoint, and then carry out the corresponding operations on the equations describing the physics.

In Fig. 13, the short circuits of Fig. 10 have been removed, and the mechanical boundary networks are also absent. We shall obtain the impedance matrix for this seven-port, and, after its validity has been established by recourse to the equations of the physical problem, use the matrix in conjunction with the mechanical networks, established in like manner, to arrive at an overall realization. This approach leads to a relatively simple analytical form for the impedance matrix of the complete network, and one which is easy to obtain, whereas inclusion of the mechanical networks and arbitrary mechanical loads at the outset greatly complicates the analysis.

Consider the posited Fig. 13. Because it pertains to normal coordinates, the port-variables are superscripted with the degree sign, as shown. The ports are numbered so that the left side (bottom of the crystal) of the transmission line supporting mode (i) leads to port (i°), while the right side (top of the crystal) of the same transmission line leads to port $((i + 3)^{\circ})$; ports (1°) to (6°) are the mechanical ports, while port (7°) is the electrical port. We also define V_{π}° and I_{π}° $(\pi = 1,2,\ldots,7)$ as the voltages and currents appropriate to port number (π°), with conventions as shown in Fig. 13. At present we do not have to match these variables with the stresses and displacements.

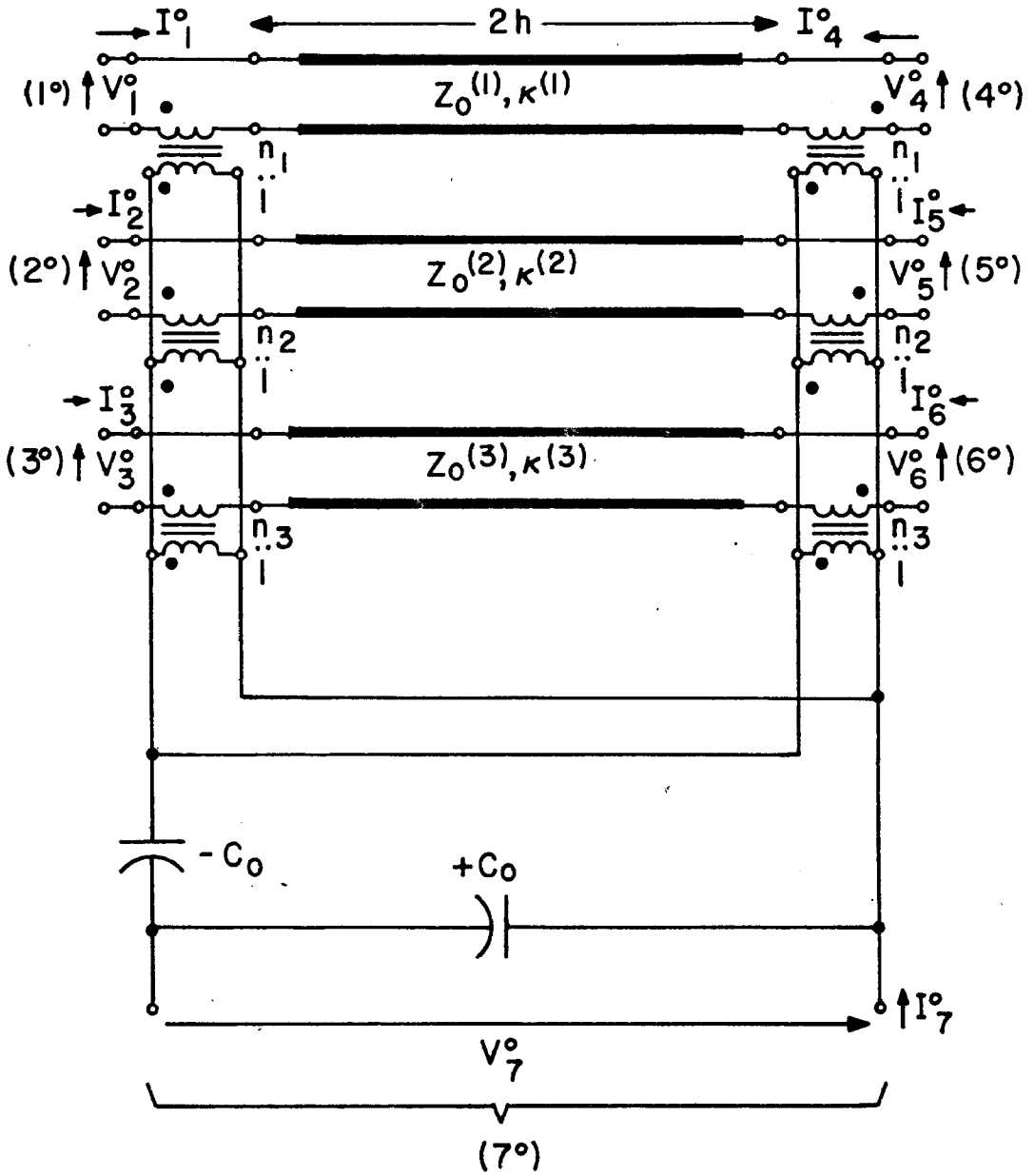

FIG. 13. SEVEN-PORT, NORMAL-MODE, EQUIVALENT CIRCUIT, WITHOUT MECHANICAL BOUNDARY NETWORKS AND LOADS.

In order to carry out the analysis of the circuit of Fig. 13, it is convenient to replace the distributed lines by their equivalent lumped tee form. This form is shown in Fig. 14 for a single line, and the substitution of three such tees for the lines in Fig. 13 produces the network of Fig. 15.

We seek to determine the quantities $z^{\circ}_{\pi\xi}$ in the relations

$$V^{\circ}_{\pi} = z^{\circ}_{\pi\xi} \; I^{\circ}_{\xi} \tag{3.23}$$

where the Greek indices have the range 1 to 7. Our task is reduced in size by a number of considerations. First, as a consequence of the fact that the network is composed of linear, passive and bilateral elements, and because we will choose our loop current definitions to coincide with our choice of loops for application of Kirchhoff's voltage law, the parameter matrices will be symmetrical (202). We notice, also, that the impedances break up into four types, viz., driving-point impedances, which are electrical or mechanical, and transfer impedances, which connect either two mechanical ports or a mechanical port to the electrical port. Apart from the mode index number, all the driving-point mechanical impedances will be equal, as will the mutual mechanical impedances between the two ports of a single transmission line. Again, mutatis mutandis, all of the electrical-mechanical transfer impedances will be equal. Finally, all of the mechanical impedances, whether driving point or transfer become almost trivially simple to evaluate by virtue of the two capacitances, which together produce a shorting of the piezo-transformers, when port (7^{O}) is open, thereby decoupling the transmission lines from each other.

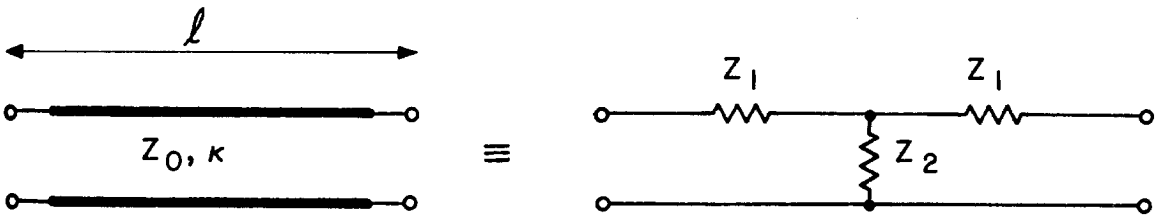

$$Z_1 = \frac{Z_0}{j \sin\theta}\,(\cos\theta - 1) = j\,Z_0 \tan(\theta/2)$$

$$Z_2 = \frac{Z_0}{j \sin\theta} \quad ; \quad \theta = \kappa\ell$$

FIG. 14. LUMPED, TEE, FORM OF A TRANSMISSION-LINE SECTION.

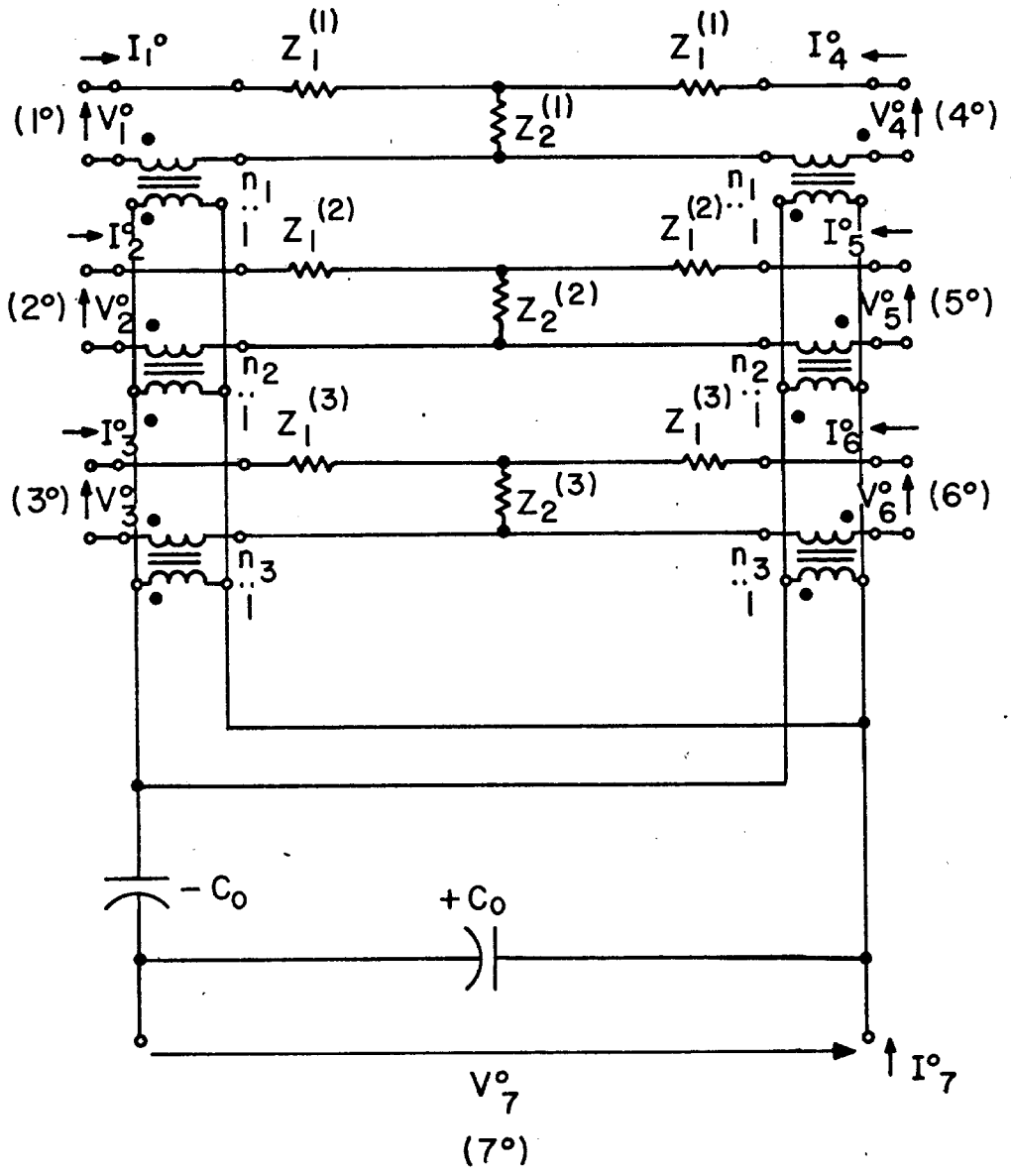

FIG. 15. LUMPED CIRCUIT FOR EVALUATING TETM ELECTRO-MECHANICAL IMPEDANCE MATRIX.

This last-mentioned consideration has the effect of making vanish the impedance matrix elements with the following indices: 12,13,15,16, 23,24,26,34,35,45,46 and 56, plus, by symmetry, those with these indices in reverse order. These correspond to mechanical transfer impedances between different lines. The mechanical driving-point impedances are

$$Z_{11}^{\circ} = Z_{44}^{\circ} = Z_1^{(1)} + Z_2^{(1)} = \frac{Z_o^{(1)}}{j \tan \theta_1} , \tag{3.24}$$

$$Z_{22}^{\circ} = Z_{55}^{\circ} = Z_1^{(2)} + Z_2^{(2)} = \frac{Z_o^{(2)}}{j \tan \theta_2} , \tag{3.25}$$

and

$$Z_{33}^{\circ} = Z_{66}^{\circ} = Z_1^{(3)} + Z_2^{(3)} = \frac{Z_o^{(3)}}{j \tan \theta_3} , \tag{3.26}$$

where we have put

$$\theta_i = 2h\chi^{(i)} . \tag{3.27}$$

The mutual mechanical impedances that are not zero, are

$$Z_{14}^{\circ} = Z_{41}^{\circ} = Z_2^{(1)} = \frac{Z_o^{(1)}}{j \sin \theta_1} , \tag{3.28}$$

$$Z_{25}^{\circ} = Z_{52}^{\circ} = Z_2^{(2)} = \frac{Z_o^{(2)}}{j \sin \theta_2} , \tag{3.29}$$

and

$$Z^{\circ}_{36} = Z^{\circ}_{63} = Z^{(3)}_{2} = \frac{Z^{(3)}_{o}}{j \sin \theta_3} . \qquad (3.30)$$

With the mechanical ports (1°) to (6°) open-circuited, the impedance seen looking into the electrical port is

$$Z^{\circ}_{77} = \frac{1}{j\omega C_o} , \qquad (3.31)$$

which is consistent with the mechanical port conditions, since we shall find that open circuits at the mechanical ports mean zero velocities and displacements, so the crystal is clamped and the piezoelectric effect is prevented from contributing to the impedance seen at port (7°).

It remains to obtain the electro-mechanical transfer impedances. We pick z°_{71} as representative. Ports (2°) through (7°) are open, so a short is placed across all piezo-transformers, decoupling the three transmission lines. A current I_1° injected into port (1°) as shown, produces a current $n_1 I_1^{\circ}$ on the primary side of the piezoelectric drive transformer. This current flows through the positive and negative capacitors and produces a voltage at port (7°) of $n_1 I_1^{\circ}/(j\omega C_o)$, polarized as shown, hence

$$Z^{\circ}_{71} = \frac{n_1}{j\omega C_o} = Z^{\circ}_{74} . \qquad (3.32)$$

Similarly one obtains

$$Z^{\circ}_{72} = \frac{n_2}{j\omega C_o} = Z^{\circ}_{75} , \qquad (3.33)$$

and

$$Z^{\circ}_{73} = \frac{\eta_3}{j\omega C_o} = Z^{\circ}_{76} . \qquad (3.34)$$

With the symmetry of the impedance matrix about the main diagonal, this completes the evaluation of the $Z^{\circ}_{\pi 5}$. The entire array is given on the next page. If instead of three modes, only one is considered, the corresponding three-port impedance matrix is obtained from our seven-port matrix by eliminating any two of the first three rows and columns, and the same members of the second set of three rows and columns, then suppressing the mode index number in what remains. With a trivial renumbering of ports, it will be seen to be identical with that given by Auld (8).

$$
[Z^{o}] = \begin{bmatrix}
\frac{Z_o^{(1)}}{j\tan\theta_1} & 0 & 0 & \frac{Z_o^{(1)}}{j\sin\theta_1} & 0 & 0 & \frac{n_1}{j\omega C_o} \\
0 & \frac{Z_o^{(2)}}{j\tan\theta_2} & 0 & 0 & \frac{Z_o^{(2)}}{j\sin\theta_2} & 0 & \frac{n_2}{j\omega C_o} \\
0 & 0 & \frac{Z_o^{(3)}}{j\tan\theta_3} & 0 & 0 & \frac{Z_o^{(3)}}{j\sin\theta_3} & \frac{n_3}{j\omega C_o} \\
\frac{Z_o^{(1)}}{j\sin\theta_1} & 0 & 0 & \frac{Z_o^{(1)}}{j\tan\theta_1} & 0 & 0 & \frac{n_1}{j\omega C_o} \\
0 & \frac{Z_o^{(2)}}{j\sin\theta_2} & 0 & 0 & \frac{Z_o^{(2)}}{j\tan\theta_2} & 0 & \frac{n_2}{j\omega C_o} \\
0 & 0 & \frac{Z_o^{(3)}}{j\sin\theta_3} & 0 & 0 & \frac{Z_o^{(3)}}{j\tan\theta_3} & \frac{n_3}{j\omega C_o} \\
\frac{n_1}{j\omega C_o} & \frac{n_2}{j\omega C_o} & \frac{n_3}{j\omega C_o} & \frac{n_1}{j\omega C_o} & \frac{n_2}{j\omega C_o} & \frac{n_3}{j\omega C_o} & \frac{1}{j\omega C_o}
\end{bmatrix}
$$

D. The TETM Plate Electromechanical Impedance Matrix

Having the matrix array for the posited Fig. 13, we now show that this same array appears from the equations governing the motion of the crystal plate, obtained in Chapter II, when the properly analogous quantities are paired. Once this has been done, an appeal to the fact that the acoustic and transmission-line waves obey the same equations of motion within the region $-h < x < h$ and have the same boundary values, will establish the fact that Fig. 13 constitutes a true analog up to the mechanical boundaries. After the mechanical boundary networks have been added, in Chapter V, the analogy for a single plate will be complete in all respects.

In keeping with (2.52) and (2.53) we adopt the choices

$$V_\pi^\circ = A\, T_{3i}^\circ(-h) , \qquad (\pi = i = 1,2,3) , \tag{3.35}$$

$$V_\pi^\circ = A\, T_{3i}^\circ(+h) , \qquad (\pi = i+3 = 4,5,6) , \tag{3.36}$$

$$V_\pi^\circ = V_7^\circ , \qquad (\pi = 7) , \tag{3.37}$$

where T_{3i}° $(\pm h)$ refers to the value of T_{3i}° at the top, resp., bottom, of the plate.

Note that the choice here pertains to the total stress T_{3i}°, and not simply to the "wavy" portion, $\tilde{T}_{3i}^\circ$.

The currents are taken as

$$I_\xi^\circ = -\dot{u}_i^\circ(-h) = -j\omega u_i^\bullet(-h), \qquad (\xi = i = 1,2,3), \tag{3.38}$$

$$I_\xi^\circ = +\dot{u}_i^\circ(+h) = +j\omega u_i^\circ(+h), \qquad (\xi = i+3 = 4,5,6), \quad (3.39)$$

$$I_\xi^\circ = I_7^\circ, \qquad (\xi = 7), \quad (3.40)$$

where, again, $u_i^\circ(\pm h)$ refers to the value of u_i° at $x_3 = \pm h$.

The reason for the sign difference between (3.38) and (3.39) is this: the transmission-line equations (2.42), (2.43) have a convention regarding the variables; the voltage and current are always measured in the same sense, and, as a wave progresses down the line, this sense does not change. On the other hand, we have chosen our port currents I_ξ°, in Fig. 13, to be always directed into the port at the terminal which is considered positive. The mechanical voltages have an unchanged sense along the transmission lines. Labeling in this manner is conventional for lumped networks, and preserves a nice symmetry between "input" and "output," but makes inevitable the reversal of signs elsewhere. It seems to us least undesirable to incorporate them, as we have done, in the distinction between (3.38) and (3.39).

Based upon these choices relating circuit variables and physical quantities, the impedance matrix elements will depend upon quotients of stress components and components of displacement, both in the normal-coordinate system.

By definition, the impedance element $Z_{\pi\xi}^\circ$ is obtained from

$$Z_{\pi\xi}^\circ = V_\pi^\circ / I_\xi^\circ, \quad (3.41)$$

with all currents equal to zero except for I_ξ°. The physical significance of having six of the seven currents equal to zero is this: since the first six currents have been taken to be proportional

to the displacement components at the bottom and top faces of the plate, in the normal coordinates, we see that if ξ is equal to seven, referring to the electrical port current, the fact that all mechanical currents are zero means the plate is completely clamped at the top and bottom surfaces, and, since the piezoelectric drive is located only there, the crystal plate cannot move. This statement parallels our remarks about the traction-free case where the stresses vanished in the normal coordinate system, because they vanished in the untransformed system, and $\beta_j^{(i)}$ is nonsingular. When ξ is not equal to seven, then only five of the six mechanical currents are zero, and only one plate surface is clamped and cannot move. The other surface has, in general, all components of motion in the untransformed system; however, these are not independent, but bear constant ratios to one another as dictated by the direction cosines of the transformation, since I_ξ^o is compounded of untransformed components of motion in the ratio of the $\beta_j^{(i)}$. This becomes more readily apparent when the impedance components are evaluated, as we now do.

As one would expect, the same conclusions we came to in the network case, regarding certain impedance components being identical save for change of mode index number, are valid here. This allows us to cut down on the number of elements to be evaluated.

Again, four categories of impedances are recognized. The first is the electrical input impedance z_{77}^o ; this differs from the reciprocal of (3.15) because, in that case, the tractions, but not the displacements, were forced to be zero. We take u_i^o (i = 1,2,3) to be identically zero everywhere. This satisfies (2.39).

Equation (2.41) becomes

$$\varphi = a_3 x_3 + b_3 \ . \tag{3.42}$$

Application of the boundary conditions (3.2) then gives

$$b_3 = 0,$$

and

$$a_3 = \varphi_0 / h \ . \tag{3.43}$$

From (2.20), (3.12), (3.43) and (3.14) we arrive at

$$Z_{77}^{\circ} = \left(V_7^{\circ} / I_7^{\circ} \right)_{u_i^{\circ}=0} = 1/j\omega C_0 . \tag{3.44}$$

The remaining impedances may be obtained by assuming one of the u_i° to be finite and the other two to be identically zero. Because the u_i° are uncoupled in the bulk, they satisfy (2.39) separately. A value of zero satisfies (2.39), and makes four of the six mechanical currents vanish. The fifth is made to vanish by chosing the finite u_i° to be a solution of (2.39) in such a manner that it is zero at the appropriate surface, and non-zero at the other. Choosing

$$u_i^{\circ} = C_i \sin \varkappa^{(i)} (h \pm x_3) \tag{3.45}$$

accomplishes this; the sign being chosen to make u_i° vanish at $x_3 = \mp h$, respectively.

For definiteness, we take

$$u_2^{\circ} = u_3^{\circ} = 0 \tag{3.46}$$

everywhere, and, as a solution to (2.39),

$$u_1^{\circ} = C_1 \sin \varkappa^{(1)} (h - x_3) \ . \tag{3.47}$$

As a consequence of the requirement that, now,

$$I_7^o = 0,$$

plus (3.12), we have

$$D_3 = 0;$$

and, by (2.20)

$$a_3 = 0,$$

so that, from (2.38), we get

$$T_{3i}^{\circ} = c^{(i)} u_{i,3}^{\circ} . \tag{3.48}$$

With (3.46) we obtain

$$T_{32}^{\circ} = T_{33}^{\circ} = 0, \tag{3.49}$$

which leads to

$$V_2^{\circ} = V_3^{\circ} = V_5^{\circ} = V_6^{\circ} = 0, \tag{3.50}$$

and, hence, the $Z_{\pi\xi}^{\circ}$ having the subscripts 21,31,51 and 61, are zero. We shall omit doing it, but it is very easily shown by changing the mode index number (i) of the u_i^o that is chosen to remain finite, that the $Z_{\pi\xi}^{\circ}$ are symmetric, so that impedance elements with subscripts 12,13,15 and 16 are also zero. It also then appears that, additionally, the following-subscripted elements vanish, along with their symmetrically-related partners: 23,24,26,34,35,45,46 and 56.

We now continue to determine the finite impedance components stemming from our choice (3.46), (3.47). Using (3.48) and (3.47)

gives

$$T_{31}^{\circ} = -\varkappa^{(1)} c^{(1)} C_1 \cos \varkappa^{(1)} (h - x_3), \tag{3.51}$$

so that, by (3.35), (3.36), and (3.27),

$$V_1^{\circ} = -\varkappa^{(1)} c^{(1)} C_1 A \cos \theta_1 , \tag{3.52}$$

and

$$V_4^{\circ} = -\varkappa^{(1)} c^{(1)} C_1 A . \tag{3.53}$$

I_1° is obtained from (3.38) and (3.47):

$$I_1^{\circ} = -j\omega C_1 \sin \theta_1 , \tag{3.54}$$

so we have determined

$$Z_{11}^{\circ} = Z_0^{(1)} / (j \tan \theta_1) , \tag{3.55}$$

plus

$$Z_{41}^{\circ} = Z_0^{(1)} / (j \sin \theta_1) , \tag{3.56}$$

and use has been made of (2.45), (2.54) and (2.56).

Making other choices for (i) in (3.45), and using both the plus and minus signs therein, for each such choice, a repetition of the steps directly above leads to

$$Z_{11}^{\circ} = Z_{44}^{\circ} = \frac{Z_0^{(1)}}{j \tan \theta_1} , \tag{3.57}$$

$$Z_{22}^{\circ} = Z_{55}^{\circ} = \frac{Z_0^{(2)}}{j \tan \theta_2} , \tag{3.58}$$

$$Z_{33}^{\circ} = Z_{66}^{\circ} = \frac{Z_o^{(3)}}{j \tan \theta_3}, \qquad (3.59)$$

which are the same as (3.24), (3.25) and (3.26); also

$$Z_{14}^{\circ} = Z_{41}^{\circ} = \frac{Z_o^{(1)}}{j \sin \theta_1}, \qquad (3.60)$$

$$Z_{25}^{\circ} = Z_{52}^{\circ} = \frac{Z_o^{(2)}}{j \sin \theta_2}, \qquad (3.61)$$

and

$$Z_{36}^{\circ} = Z_{63}^{\circ} = \frac{Z_o^{(3)}}{j \sin \theta_3}. \qquad (3.62)$$

These are the same as (3.28), (3.29) and (3.30), while (3.44) is the same as (3.31).

All but the electro-mechanical transfer impedances have been obtained; this calculation follows next.

Once again we use (3.46), (3.47), and compute the voltage developed across the open electrical port. For the same reasons given following (3.47), a_3 is again zero, while the quantity b_3 is of no concern because it does not enter the expression for V_7°, which is

$$V_7^{\circ} = \left[\varphi(x_3 = +h) - \varphi(x_3 = -h) \right], \qquad (3.63)$$

$$V_7^{\circ} = \left[u_1^{\circ}(+h) - u_1^{\circ}(-h) \right] e_{313}^{\circ} / \epsilon_{33}^{S}; \qquad (3.64)$$

this last expression following from (2.41) with $a_3 = 0$ and the choices (3.46), (3.47) for the u_i^o. Substituting the particular form for u_1^o given by (3.47) makes V_7^o become

$$V_7^o = - C_1 \, e_{313}^o \sin\theta_1 \, / \epsilon_{33}^S \, . \tag{3.65}$$

The current I_1^o is obtained from (3.54), so the impedance z_{71}^o is

$$Z_{71}^o = e_{313}^o \, / (j\omega \, \epsilon_{33}^S) \, . \tag{3.66}$$

Recalling the definitions (3.14) and (3.17) allows us to put this in the form

$$Z_{71}^o = \frac{n_1}{j\omega \, C_o} \, , \tag{3.67}$$

which is seen to agree with (3.32).

Continuing exactly as we have proceeded above to determine z_{71}^o, but with interchanges of index numbers, one may similarly show that

$$Z_{71}^o = Z_{74}^o = \frac{n_1}{j\omega \, C_o} \, , \tag{3.68}$$

$$Z_{72}^o = Z_{75}^o = \frac{n_2}{j\omega \, C_o} \, , \tag{3.69}$$

and

$$Z_{73}^o = Z_{76}^o = \frac{n_3}{j\omega \, C_o} \, . \tag{3.70}$$

These relations are identical with (3.32), (3.33) and (3.34). The

symmetry of the $Z^{\circ}_{\pi\xi}$ about the main diagonal makes the determination complete, and, it is seen that our assignments (3.35) to (3.40) are, in every respect, consistent with the posited Fig. 13 and with the equations governing the physics of the system, so that the impedance matrices obtained from the physics and the figure are identical. The impedance matrix is further seen to have the property that all mechanical ports are on an equal footing, the only difference being the arbitrarily assigned port numbers; this property also follows at once from Fig. 13.

This section has developed the seven-port impedance matrix from the physical equations governing the problem. Upon comparison with the matrix of Section C, one sees they are identical. This justifies not only our choice of pairings of variables between the circuit and the problem, but proves that Figure 13 is an exact representation of the physical problem as seen at the ports (π^0). We remark again that the complete problem involves additional circuitry, so that the mechanical conditions at the layer surfaces can be expressed in untransformed variables, instead of those superscripted with the degree sign. Within the normal-coordinate framework, however, the representation of Figure 13 is exact. One additional topic remains to be considered yet, and this concerns the piezoelectric drive, to which we devote the next section. We mention in passing that we have marked out upon our unbounded plate a portion of area A and have characterized this; the entire plate is simply more such areas, with all of them in parallel. It will be noticed that the LETM case treated in Chapter IV presents the dual situation

of portions of a single plate characterized as being in series electrically.

E. Piezoelectric Tractions.

We noted in Section IB 5. the historical development of the concept of piezoelectric tractions taking place at discontinuities. In this regard, Holland's work (102) deserves special mention as it pertains to piezo-vibrators and stacks of plates, and he emphasized the surface-traction aspect in these situations.

We have arrived, in our work, at circuit representations which place just such an interpretation in evidence. That is, our circuits portray the piezo-drive effect as a phenomenon that takes place at the surfaces of the plate, and therefore the schematic shares this accordance with the nature of the physical problem.

This section discusses the drive mechanism further and leads up to a demonstration that the circuits, such as those of Fig. 10 and 13, are true analogs; they provide realizations not only at the seven ports, but are valid within the bulk of the layer, as well.

The physical reason for the location of the piezo-drive transformers at the layer boundaries can be seen as follows. Newton's equations (2.1), transformed to normal coordinates, are

$$F_i^{\circ} = T_{3i,3}^{\circ} = \rho \ddot{u}_i^{\circ} \quad , \tag{3.71}$$

where the F_i° are components of mechanical force density. The F_i° arise from the differentiation of the stresses, which from (2.38), are

$$T_{3i}^{\circ} = c^{(i)} u_{i,3}^{\circ} + e_{33i}^{\circ} a_3 \ . \tag{2.38}$$

The quantity a_3, in turn, is a uniform electric field, from (2.41), which depends for its value upon the boundary conditions imposed (see, e.g., (3.6), (3.43) and above (3.48)). Differentiation of (2.38) yields no contribution from the second term on the right within the bulk of the crystal, where $e^{\circ}_{33i}\, a_3$ is constant. However, each surface produces a discontinuity, so the differentiation yields a delta-function of force density, located at the surface. This will, in general, result in all three components of F°_i being produced there. In the event that the material comprising the plate is not piezoelectrically homogeneous, additional contributions to F°_i will be produced because the term $a_3\, e^{\circ}_{33i,3}$ is then not always zero. We do not consider this further, but it may be treated by the method set forth in Chapter VI.

The delta-functions of piezoelectric force density are represented by our transformers, which are located at the surface and exert finite forces, but have no spatial extensions.

The mechanical variables, represented by (3.35), (3.36), (3.38) and (3.39) as port voltages V°_{π} and port currents I°_{π} occur at the surfaces $x_3 = \pm h$, as do the piezoelectric drive terms discussed above. Therefore, making use of (2.47) and (2.52),

$$V^{(i)}\,(\text{at port}\,(\pi^{\circ})) = (V^{\circ}_{\pi} - A\bar{T}^{\circ}_{3i}) = A\tilde{\bar{T}}^{\circ}_{3i}\,. \qquad (3.72)$$

Also, from (2.53) and (2.38), (2.39),

$$I^{(i)}\,(\text{at port}\,(\pi^{\circ})) = I^{\circ}_{\pi} = -j\omega u^{\circ}_i\,, \quad (\pi = 1,2,3), \qquad (3.73)$$

and

$$I^{(i)}(\text{at port}(\pi^\circ)) = -I_\pi^\circ = -j\omega u_i^\circ, \quad (\pi = 4,5,6). \tag{3.74}$$

Since $V^{(i)}$ and $I^{(i)}$ are the transmission-line variables, these are then expressed directly in terms of known values at the surface. The boundary values at the transmission-line ends, expressed by (3.72), (3.73) and (3.74), are the same as those appearing at the plate surface in the physical problem. This, plus the fact that the network and the acoustic problem obey the same transmission-line equations within the bulk, as shown in Chapter II, guarantees that the network is a true analog, and that corresponding quantities are matched on a point-for-point basis along the spatial coordinate from -h to +h.

In the results of Chapter V we shall obtain suitable mechanical boundary networks to be attached to Fig. 13, which will then become complete.